Science and Technology Indonesia
e-ISSN:2580-4391 *p*-ISSN:2580-4405
Vol. 10, No. 1, January 2025

Research Paper

Micro-Magnetic Activity of the Fabricated $MnFe_2O_4$ via Co-Precipitation from Natural Iron Sand

Martha Rianna[1*], Muhammad Khalid Hussain[2,3], Timbangen Sembiring[1], Herwati Permata Indah Raja Guk-Guk[1], Kurnia Jesiska Sitorus[1], Eko Arief Setiadi[4], Anggito P. Tetuko[4], Perdamean Sebayang[4]

[1]*Department of Physics, Universitas Sumatera Utara, Medan, 20155, Indonesia*
[2]*Department of Physics, Faculty of Science, University of Gujrat, HH Campus, Gujrat, 50700, Pakistan*
[3]*Department of Physics, Faculty of Science, University of Gujrat, Sub-Campus Mandi, Bahauddin, 50400, Pakistan*
[4]*Research Center for Advanced Materials, National Research and Innovation Agency (BRIN), Tangerang Selatan, 15314, Indonesia*
***Corresponding author**: martharianna@usu.ac.id

Abstract
This study explores the micromagnetic behaviour of $MnFe_2O_4$ derived from natural iron sand through the coprecipitation method, without the need for calcination. Using manganese chlo-ride and iron sand as precursors, one can create $MnFe_2O_4$. Through the utilisation of X-ray Diffraction (XRD), Scanning Electron Microscope-Energy Dispersive X-Ray (SEM-EDX), and Vibrating Sample Magnetometer (VSM), one can effectively analyse and understand the crystal structure, morphology, and magnetic properties. The crystal size was reduced by a fac-tor of 0.40 nm, as revealed by XRD crystal structure analysis. Additionally, the XRD results indicated the absence of impurities, confirming the presence of a single phase. In addition, the SEM analysis revealed that samples 1, 2, and 3 underwent agglomeration. The particles have a cubic shape. The analysis using EDX indicates that there are no other elements present in the Mn, Fe, and O. Additionally, the VSM analysis confirms that the sample exhibits magnetic hardness. Sample 1 exhibits exceptional magnetic properties, with Ms values of 217.53 emu/g, Mr 34.27 emu/g, and Hc 127.42 emu/g. Photoluminescence (PL) spectroscopy was used to observe the optical properties of $MnFe_2O_4$. Sample 1 exhibits a distinct emission spectrum at 440 nm, representing the purple band. Sample 2 displays a sharp emission spectrum at 448 nm, indicating the blue band. Lastly, Sample 3 demonstrates a clear emission spectrum at 427 nm, signifying the purple band.

Keywords
$MnFe_2O_4$, Co-Precipitation Method, Morphology, Crystal Structure, Magnetic Properties

Received: 31 July 2024, Accepted: 3 December 2024
https://doi.org/10.26554/sti.2025.10.1.221-227

1. INTRODUCTION

Research and application of nanotechnology have developed rapidly in the last decade. Magnetic materials have attracted attention. The manufacture of $MnFe_2O_4$ has been carried out for many applications such as MRI (Ravichandran and Velumani, 2020), removal of clean water (Thy et al., 2020), catalysis (Qin et al., 2020), antibiotics degradation (Dieu Cam et al., 2021), etc. The chemical synthesis and presence of multivalent metal ions in its spinel structure give $MnFe_2O_4$ its significance. This compound, $MnFe_2O_4$, falls under the category of inverse spinel ferrites. In this structure, both Mn^{2+} and Fe^{2+} ions are found in the tetrahedral sites, while Fe^{3+} ions are located in the octahedral sites (Arun et al., 2020). Similar to a physical chemist, one can observe an enhancement in electronic conductivity when transitioning be-tween divalent and trivalent ions in the inverse spinel structure during the redox reaction pro-cess. Because it is possible to adjust experimental parameters such reaction temperature, time, proportion of oxidation or reducing agent, and addition of nucleating agent, the chemical oxi-dation process plays an essential and appealing role in the synthesis of $MnFe_2O_4$.

Previous research was conducted about $MnFe_2O_4$ for various purposes. Peng et al. (2023) added rGO in $MnFe_2O_4$ as composite rGO/$MnFe_2O_4$ with the chemical process for electrical heating and mi-crowave absorbing material. With a thickness of 3 mm and a reflection loss of 43.2 dB at 14.1 GHz at 800°C, the resistance that results is 19.18 Ω. $MnFe_2O_4$ doped Zn and Dy in their re-spective magnetic and structures. Shayestefar et al. (2022) prepara-tion and characterization of $MnFe_2O_4$ doping Zn and Dy in structure and magnetic properties, respectively. The study found that the crystal size and magnetic saturation ranges are 13 to 30 nm and 30 to 67 emu/g, respectively. Kumar et al. (2022) are doing a syn-thesis

of $MnFe_2O_4$ coating PEG-2000, respectively. The crystallite size results in the range of 36-45 nm and saturation magnetization of 68 emu/g. Amulya et al. (2021) reported the synthesis of $MnFe_2O_4$ nano-particles using sono-chemical. It is crystallite size results in the range of 16-24 nm. Correspondingly, influences of Mn in Fe_3O_4 materials in-crease structural and magnetic properties (Abdullah et al., 2023; de Góis et al., 2022).

Based on this literature, we present first time in this research the micro-magnetic activity of $MnFe_2O_4$ in permanent magnetic materials using a co-precipitation approach and without cal-cination temperatures. These syntheses use natural iron sand and manganese chloride as main precursors. The characterizations were carried out using X-Ray Diffraction, Scanning Electron Microscopy, and Energy Dispersive X-Ray, Vibrating Sample Magnetometer, and Photoluminescence (PL).

2. EXPERIMENTAL SECTION

2.1 Materials and Instrumentation

The main precursor's manganese chloride (Mecrk), natural iron sand NaOH (Merck), HCl 37% (Merck), Whatman filter paper, hot plate, magnetic stirrer. It was carried out in this research using the co-precipitation approach. The mass ratio that will be used as shown in the Table 1.

Table 1. Comparison of Manganese Chloride and Natural Iron Sand

Sample Code	Manganese Chloride: Natural Iron Sand
1	4: 6
2	5: 5
3	3: 7

The characterization using X-Ray Diffraction (XRD) Smartlab. The morphology of $MnFe_2O_4$ was tested using Scanning Electron Microscope-Energy Dispersive X-Ray Spectroscopy (SEM-EDX) Hitachi. To determine the magnetic properties of $MnFe_2O_4$ tested using Vibrat-ing Sample Magnetometer (VSM) DXV-9000 and the optical properties using photolumines-cence (PL) Horiba.

2.2 Methods

The manganese chloride material was ground using a mortar cup, then the Iron Sand was sifted through a 120 mesh sieve and then weighed with the required mass in grams. In addition to the standard materials above, NaOH (1M) is also necessary as a precipitate in the artificial process & aqua dest as a solvent. The synthesis was carried out by mixing 4 grams of Fe_2O_4, and 50 mL of HCL (37%) and stirring for 30 minutes, and then the solution was filtered using Whatman filter paper. The filter solution was mixed by adding 6 grams of MnCl, then started using a magnetic bar on a hot plate for 30 minutes. Then add the re-solution to 150 mL of NaOH (1M) solution slowly drop by drop while stirring using a magnetic bar on a hot plate at a speed of 700 rpm and 180° for 2 hours. Then the washing process is carried out using Aquades and ethanol to neutralize the pH and remove the salts formed during the reaction. If a precipitate form at the bottom of the beaker, then the water in the beaker is removed carefully using a dropper so that the sediment is not wasted. Washing was carried out on a scheduled basis until the precipitate formed had a neutral pH. Then dried using an electric roast at a temperature of T = 250 with a time of t = 2 hours. The dried precipitate is then ground and ground as a powder. The sample in the form of a fine powder was then dryed at a temperature of 200 for 2 hours. To determine the microstructure of $MnFe_2O_4$ tested with X-Ray Diffraction (XRD). The morphology of $MnFe_2O_4$ was tested using Scanning Electron Microscope-Energy Dispersive X-Ray Spectroscopy (SEM-EDX). To determine the magnetic properties of $MnFe_2O_4$ tested using Vibrating Sample Magnetometer (VSM) and the optical properties using Photoluminescence (PL).

3. RESULTS AND DISCUSSION

3.1 Structural of $MnFe_2O_4$

Several diffraction patterns, characteristic peaks of a sample, are tested by X-Ray Diffraction (XRD). XRD testing was carried out to determine the phase formed, the highest peak, and the crystal structure of $MnFe_2O_4$ with composition variations in Figure 1 and Table 2.

Table 2. Crystal Parameters at Miller Index 311

Sample Code	2θ (deg)	Intensity (a.u)	FWHM	Crystal Diameter (nm)
1	35.72	173.16	0.56	0.51
2	35.72	174.66	0.57	0.13
3	35.53	174.06	0.58	0.40

XRD diffraction patterns are plotted in 2D graphs, namely x and y, where the x-axis is the diffraction angle, and the y-axis is the peak intensity. Each peak in the diffraction pattern oc-curs due to X-rays reflected from the plane against the XRD-tested sample. The positions of the peaks have different intensities depending on the crystal structure, this is evident from the appearance of diffraction peaks with Miller indices (111), (220), (311), (420), (551), (440) and (620), which is the spinel cubic structure of $MnFe_2O_4$.

Based on the analysis of the data from Table 2, using the Scherrer equation, the crystal grain size shown in the Table 2 is obtained for the sample $MnFe_2O_4$ composition 4:6 (sample 1) 0.5102 nm and $MnFe_2O_4$ composition 5:5 (sample 2) 0.13 nm and a 3:7 compositions (sample 3) 0.400 nm. As seen in Figure 1 in sample 3, there is a peak shift due to differences in com-position variations resulting in a decrease in the intensity value and an increase in the FWHM value. Grid parameter value increased due to the difference in the radius of Mn (1.72) com-pared to Fe (0.67) (Al-Zahrani et al., 2022). This is caused by the heating process and the dif-ference in the ratio of

Table 3. Magnetic Properties of $MnFe_2O_4$ with Variation Compositions

Sample Code	Ms (emu/g)	Mr (emu/g)	Hc (Oe)	B ($\times 10^9$ Oe2)	k_1
1	217.53	34.27	127.42	0.96	0.96
2	208.78	33.63	113.41	0.81	0.99
3	30.46	6.86	118.70	0.95	0.99

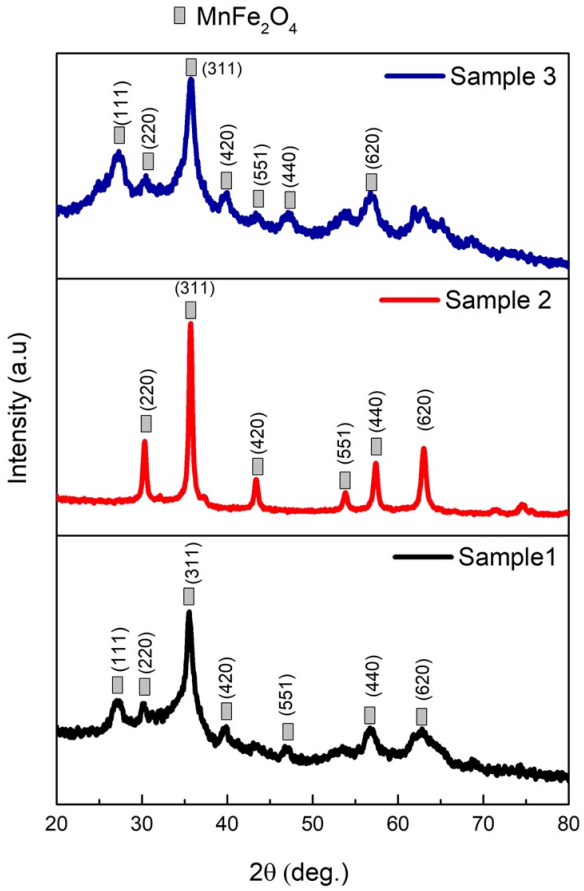

Figure 1. Diffraction pattern of $MnFe_2O_4$

faithful samples (Akhlaghi and Najafpour-Darzi, 2021; Cheng and Ji, 2024; Kalaiselvan et al., 2022). Table 2 shows that the height of the intensity peak identifies the crystal size of a sample. From the Deybe Scherrer equation, it shows that the grain size value produced will be inversely proportional to the FWHM value, while the FWHM value is influ-enced by the intensity of each crystal plane, where the higher the intensity, the smaller the FWHM value (Sukmarani et al., 2020). The wider the FWHM value, the better the atomic order. From the results of this XRD test, it does not have impurities because it has been con-firmed that the single phase is seen in the EDX results. This proves that $MnFe_2O_4$ has a high degree of crystallinity.

3.2 Morphology of $MnFe_2O_4$

To analyze the morphological structure of a material, characterization was carried out using Scanning Electron Microscopy (SEM). Through the SEM test, the microstructure and particle size of the manganese ferrite material can be known. Microstructure observations of the $MnFe_2O_4$ magnetic powder were carried out using the SEM-EDX in Figure 2 and Figure 3.

The images on samples 1,2 and 3 each at 1000× magnification which has a surface morphology with random particles from the smallest particle size to the largest particle size. From the his-togram in Figure 2, it can be observed that the effect of increasing the ratio of manganese and iron sand makes the particle size around 120-280 nm. Sample 1 for particle size is shown in the range of 140-280 nm, then the particle size of sample 2 is shown in the range of 120 -170 nm and the particle size in sample 3 is shown in the range of 120-220 nm. The difference in particle size affects the addition of manganese and ferrite (Sharifi et al., 2021). The EDX spectrum is depicted in Figure 3, which includes components such as manganese, iron, and oxygen. The resulting atomic weight percentage and atomic percentage are shown for each particular operation.

3.3 Magnetic Properties of $MnFe_2O_4$

Using a Vibrating Sample Magnetometer, the samples were conducted to determine the mag-netic characteristics of $MnFe_2O_4$. The hysteresis curve in Figure 4 below illustrates the strength of the material's magnetic characteristics. From this angle, one can observe the coercivity (Hc), remanent magnetisation (σr), and magnetisation magnitude (σs).

Figure 4 shows a change in the hysteresis curve's shape, indicating a change in magnetic prop-erties. Previous research by López-Ortega et al. (2015) states that permanent magnetic materials are declared for all particle sizes above 40 nm. From the results of this study, the value of coercivity tends to decrease, as in Table 3. The anisotropy parameter can be determined by $B = H_c^2/15$, where Ha is the magnetic field, and the magnetocrystalline constant (k_1) can be defined as $k_1 = 1\text{-}\mu_o M_s H_c$ (Al-Zahrani et al., 2022; Bhandare et al., 2020; Westerstrand et al., 1975). Soft magnetic material and hard magnetic material are magnetic materials that have different characteristics (Herrmann, 1991; Iusipova, 2022). Hard magnetic material is a magnetic material that still retains its magnetic properties after being magnetized, is called a permanent magnet, and has a coercivity greater than 125.6 Oe (Li et al., 2012). While soft magnetic properties are a material that is easy to magnetize but also easy to lose its magnetism after it is not magnetized, this

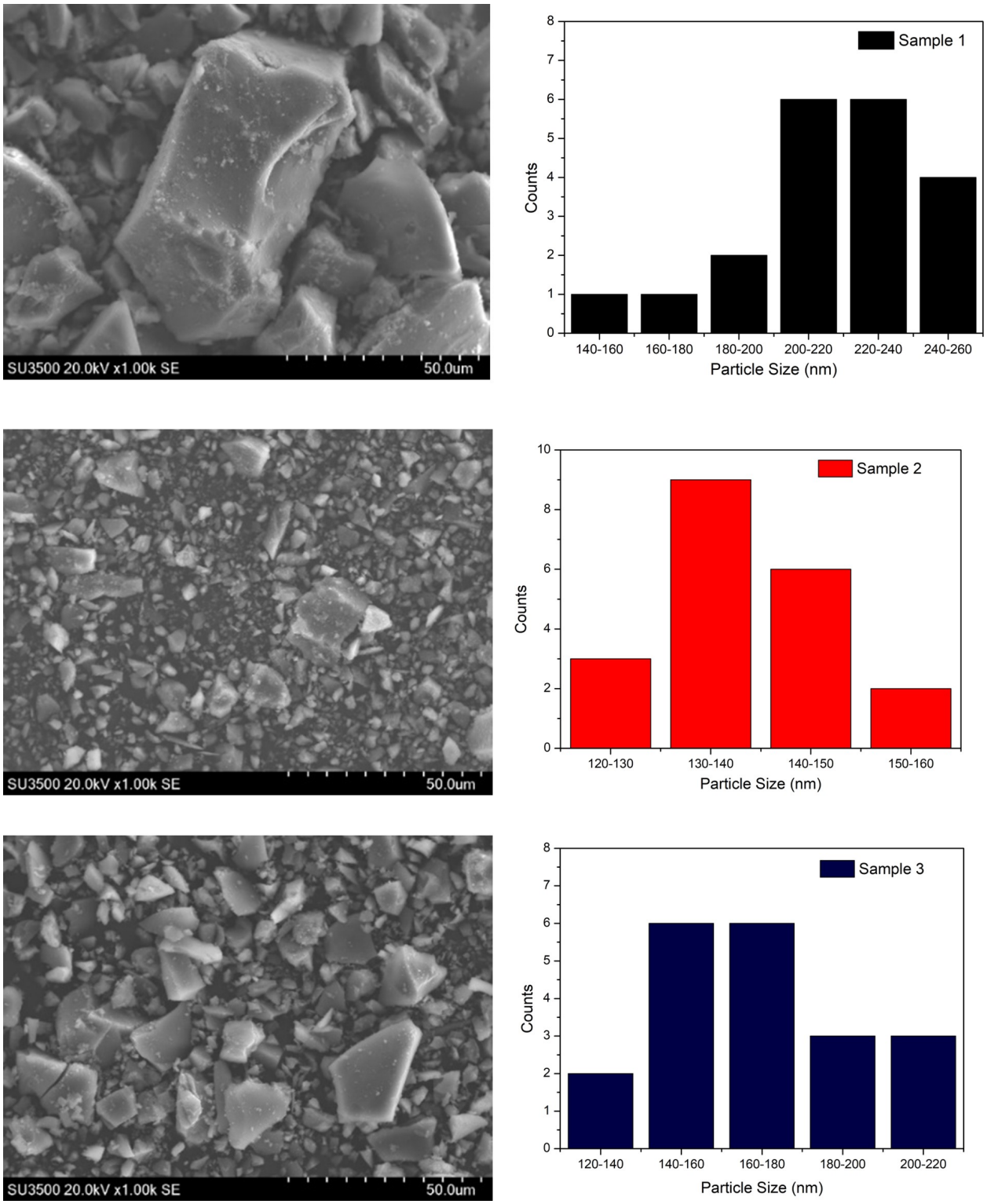

Figure 2. Morphological Results and Distribution Particle Size of $MnFe_2O_4$

material has a coercivity of less than 12.56 Oe (Chakradhary and Akhtar, 2020; Qu et al., 2022; Sharifianjazi et al., 2020). The coercivity ob-tained from the research is a hard magnetic and permanent magnetic material, respectively.

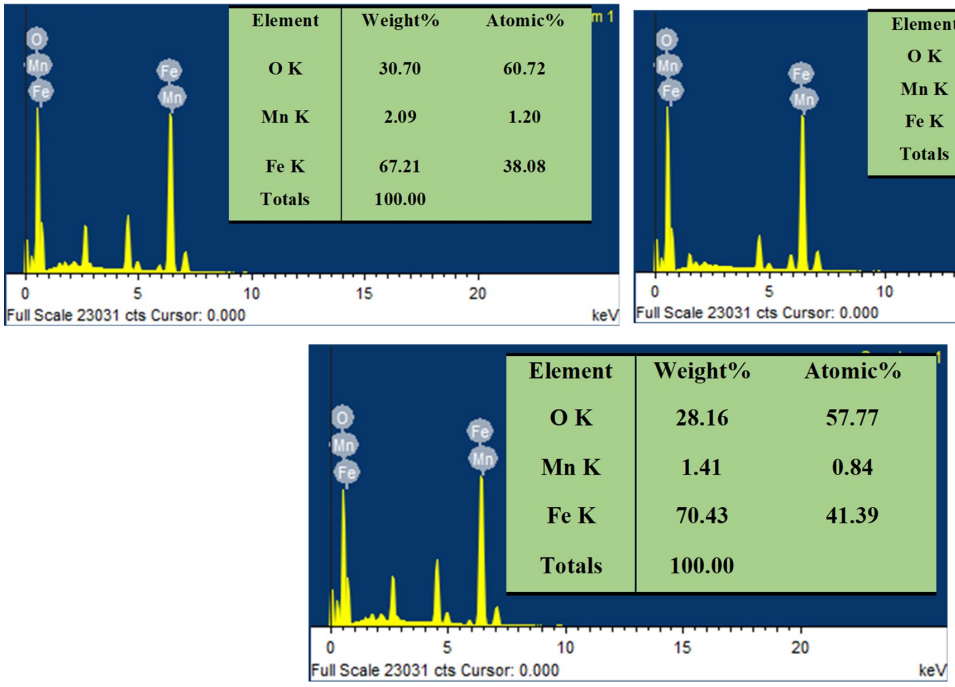

Figure 3. EDX Spectrum with Various Compositions

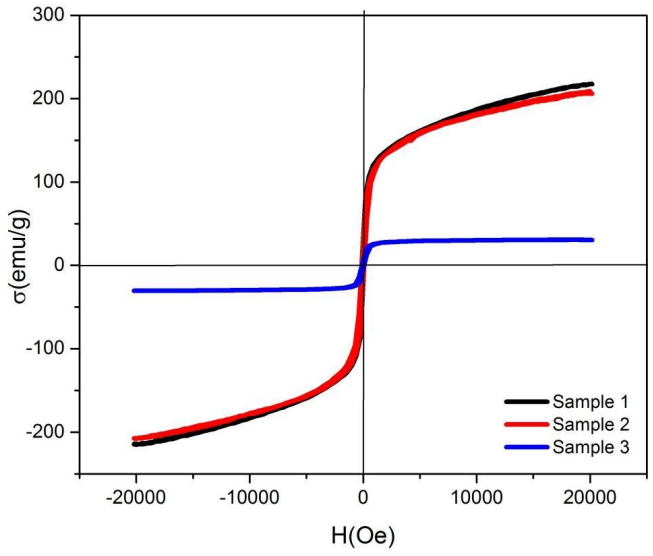

Figure 4. Hysteresis Loop of Variation Composition

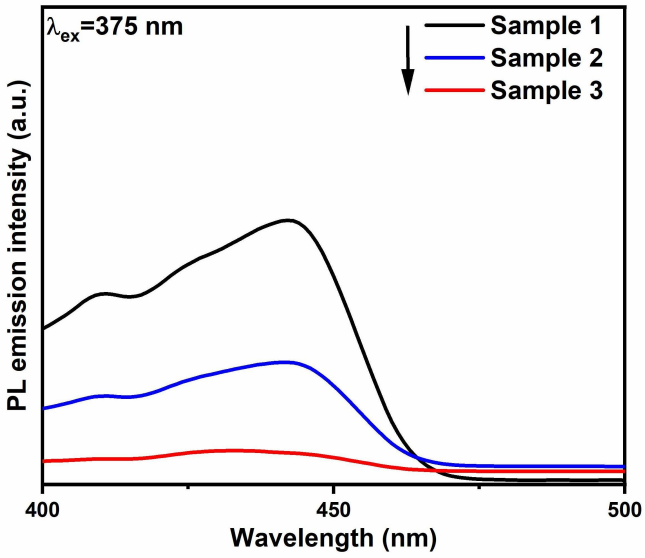

Figure 5. Photoluminescence Results of Variation Compositions

3.4 Optical Properties of $MnFe_2O_4$

Figure 5 shows optical properties of all sample synthesized with PL (Photoluminescence). These results suggest that Sample 1 is showing sharp emission spectra at 440 nm, matching to the purple band, Sample 2 at 448 nm, corresponding to the blue band, and Sample 3 at 427, matching to the purple band.

4. CONCLUSIONS

Using the coprecipitation method without calcination, this research aims to synthesise the micromagnetic activity of $MnFe_2O_4$ from natural iron sand. Using manganese chloride and iron sand as precursors, one can synthesise $MnFe_2O_4$. Characterising the crystal structure, morphology, and magnetic prop-

erties involved the use of X-ray Diffraction (XRD), Scanning Electron Microscope-Energy Dispersive X-Ray (SEM-EDX), and Vibrating Sample Magnetometer (VSM). The XRD analysis revealed a cubic crystal shape and crystal size values that aligned with the SEM characterisation results of the $MnFe_2O_4$ sample. Additionally, the particles exhibited a tendency to clump together. This study discovered hard magnetic materials and permanent magnetic materials. Photoluminescence (PL) spectroscopy was used to observe the optical properties of $MnFe_2O_4$. Sample 1 exhibits a distinct emission spectrum at 440 nm, rep-resenting the purple band. Sample 2 displays a clear emission spectrum at 448 nm, representing the blue band. Lastly, Sample 3 demonstrates a sharp emission spectrum at 427 nm, also corresponding to the purple band. The findings are suitable for producing materials with long-lasting magnetic properties.

5. ACKNOWLEDGMENT

This research is supported by Universitas Sumatera Utara from World Class University Program in Research of Scientific Cluster with Contract Number: 14/UN5.2.3.1/PPM/KP-WCU-B2/2022, University of Gujrat, and Advanced Characterization Laboratories Serpong, National Research and Innovation Agency through E-Layanan Sains, Badan Riset dan Inovasi Nasional (BRIN).

REFERENCES

Abdullah, M., F. F. Alharbi, R. Y. Khosa, H. A. Alburaih, S. Manzoor, A. G. Abid, H. E. Ali, M. S. Waheed, M. N. Ansari, and H. M. T. Farid (2023). Partial Sulfur Doping Induced Variation in Morphology of $MnFe_2O_4$ with Enhanced Electrochemical Performance for Energy Storage Devices. *Korean Journal of Chemical Engineering*, **40**(6); 1518–1528

Akhlaghi, N. and G. Najafpour-Darzi (2021). Manganese Ferrite ($MnFe_2O_4$) Nanoparticles: From Synthesis to Application - A Review. *Journal of Industrial and Engineering Chemistry*, **103**; 292–304

Al-Zahrani, S. A., A. Manikandan, K. Thanrasu, A. Dinesh, K. K. Raja, M. A. Almessiere, Y. Slimani, A. Baykal, S. Bhuminathan, S. R. Jayesh, J. Ahmed, H. S. Alorfi, M. A. Hussein, I. Khan, and A. Khan (2022). Influence of Ce^{3+} on the Structural, Morphological, Magnetic, Photocatalytic and Antibacterial Properties of Spinel $MnFe_2O_4$ Nanocrystallites Prepared by the Combustion Route. *Crystals*, **12**(2); 268

Amulya, M. A. S., H. P. Nagaswarupa, M. R. A. Kumar, C. R. Ravikumar, and K. B. Kusuma (2021). Sonochemical Synthesis of $MnFe_2O_4$ Nanoparticles and Their Electrochemical and Photocatalytic Properties. *Journal of Physics and Chemistry of Solids*, **148**; 109661

Arun, T., T. Kavin Kumar, R. Udayabhaskar, M. J. Morel, G. Rajesh, R. V. Mangalaraja, and A. Akbari-Fakhrabadi (2020). Size Dependent Magnetic and Capacitive Performance of $MnFe_2O_4$ Magnetic Nanoparticles. *Materials Letters*, **276**; 128240

Bhandare, S. V., R. Kumar, A. V. Anupama, H. K. Choudhary, V. M. Jali, and B. Sahoo (2020). Mechanistic Insights into the Sol-Gel Synthesis of Complex (Quaternary) Co-Mn-Zn-Spinel Ferrites: An Annealing Dependent Study. *Ceramics International*, **46**(11); 17400–17415

Chakradhary, V. K. and M. J. Akhtar (2020). Highly Coercive Strontium Hexaferrite Nanodisks for Microwave Absorption and Other Industrial Applications. *Composites Part B: Engineering*, **183**; 107667

Cheng, L. and Y. Ji (2024). Photocatalytic Activation of Sulfite by N-Doped Porous Biochar/$MnFe_2O_4$ Interface-Driven Catalyst for Efficient Degradation of Tetracycline. *Green Energy and Environment*, **9**(3); 481–484

de Góis, M. M., L. W. de Alencar Souza, C. H. N. Cordeiro, I. B. T. da Silva, and J. M. Soares (2022). Study of Morphology and Magnetism of $MnFe_2O_4$-Si_2 Composites. *Ceramics International*, **49**; 11552–11562

Dieu Cam, N. T., H. D. Pham, T. D. Pham, T. T. Thu Phuong, C. Van Hoang, M. H. Thanh Tung, N. T. Trung, N. T. Huong, and T. T. Thu Hien (2021). Novel Photocatalytic Performance of Magnetically Recoverable $MnFe_2O_4$/$BiVO_4$ for Polluted Antibiotics Degradation. *Ceramics International*, **47**(2); 1686–1692

Herrmann, F. (1991). Teaching the Magnetostatic Field: Problems to Avoid. *American Journal of Physics*, **59**(5); 447–452

Iusipova, I. (2022). Precession Frequency and Switching Time of the Magnetization Vector in the Spin-Valve Active Layer with Perpendicular Anisotropy. *IEEE Magnetics Letters*, **13**; 1–5

Kalaiselvan, C. R., S. S. Laha, S. B. Somvanshi, T. A. Tabish, N. D. Thorat, and N. K. Sahu (2022). Manganese Ferrite ($MnFe_2O_4$) Nanostructures for Cancer Theranostics. *Coordination Chemistry Reviews*, **473**; 214809

Kumar, P., S. Pathak, K. Jain, A. Singh, G. A. Basheed, and R. P. Pant (2022). Low-Temperature Large-Scale Hydrothermal Synthesis of Optically Active PEG-200 Capped Single Domain $MnFe_2O_4$ Nanoparticles. *Journal of Alloys and Compounds*, **904**; 163992

Li, X., K. T. Chau, M. Cheng, and W. Hua (2012). Comparison of Magnetic-Geared Permanent-Magnet Machines. *Progress in Electromagnetics Research*, **133**; 177–198

López-Ortega, A., E. Lottini, C. D. J. Fernández, and C. Sangregorio (2015). Exploring the Magnetic Properties of Cobalt-Ferrite Nanoparticles for the Development of a Rare-Earth-Free Permanent Magnet. *Chemistry of Materials*, **27**(11); 4048–4056

Peng, T., Y. Si, J. Qian, Z. Zhang, X. Yan, C. Zhu, and X. Hong (2023). Reduced Graphene Oxide/M-nFe_2O_4Nanocomposite Papers for Fast Electrical Heating and Microwave Absorption. *Applied Surface Science*, **613**; 156001

Qin, H., H. Cheng, H. Li, and Y. Wang (2020). Degradation of Ofloxacin, Amoxicillin and Tetracycline Antibiotics Using Magnetic Core-Shell $MnFe_2O_4$@C-NH_2 as a Heterogeneous Fenton Catalyst. *Chemical Engineering Journal*, **396**;

125304
Qu, C., Z. Ge, C. Yang, and X. Wang (2022). Optimization and Simulation of Auxiliary Magnetic Barrier Permanent Magnet Synchronous Machine for Wind Turbine. *Distributed Generation and Alternative Energy Journal*, **37**(3); 501–524
Ravichandran, M. and S. Velumani (2020). Manganese Ferrite Nanocubes as an MRI Contrast Agent. *Materials Research Express*, **7**(1); 016107
Sharifi, S., K. Rahimi, and A. Yazdani (2021). Highly Improved Supercapacitance Properties of $MnFe_2O_4$ Nanoparticles by MoS_2 Nanosheets. *Scientific Reports*, **11**(1); 8378
Sharifianjazi, F., M. Moradi, N. Parvin, A. Nemati, A. Jafari Rad, N. Sheysi, A. Abouchenari, A. Mohammadi, S. Karbasi, Z. Ahmadi, A. Esmaeilkhanian, M. Irani, A. Pakseresht, S. Sahmani, and M. Shahedi Asl (2020). Magnetic $CoFe_2O$ Nanoparticles Doped with Metal Ions: A Review. *Ceramics International*, **46**(11); 18391–18412
Shayestefar, M., A. Mashreghi, S. Hasani, and M. Taghi Rezvan (2022). Optimization of the Structural and Magnetic Properties of $MnFe_2O_4$ Doped by Zn and Dy Using Taguchi Method. *Journal of Magnetism and Magnetic Materials*, **541**; 168390
Sukmarani, G., R. Kusumaningrum, A. Noviyanto, F. Fauzi, A. M. Habieb, M. I. Amal, and N. T. Rochman (2020). Synthesis of Manganese Ferrite from Manganese Ore Prepared by Mechanical Milling and Its Application as an Inorganic Heat-Resistant Pigment. *Journal of Materials Research and Technology*, **9**(4); 8497–8506
Thy, L. T. M., N. H. T. My, H. H. P. Tuong, C. V. Chi, T. H. Tu, H. K. P. Ha, H. M. Nam, M. T. Phong, and N. H. Hieu (2020). Synthesis and Adsorption Ability of Manganese Ferrite/Graphene Oxide Nanocomposites for Arsenic(V) Removal from Water. *Vietnam Journal of Chemistry*, **58**(3); 287–291
Westerstrand, B., P. Nordblad, and L. Nordborg (1975). The Magnetocrystalline Anisotropy Constants of Iron and Iron-Silicon Alloys. *Physica Scripta*, **11**(6); 383

